

Shock wave–inertial microbubble interaction: A theoretical study based on the Gilmore formulation for bubble dynamics

Songlin Zhu and Pei Zhong^{a)}

Department of Mechanical Engineering and Materials Science, Duke University, Durham, North Carolina 27708

(Received 20 April 1999; accepted for publication 13 July 1999)

The Gilmore formulation for bubble dynamics coupled with zeroth-order gas diffusion were used to investigate theoretically the cavitation activity produced by a modified XL-1 lithotripter [J. Acoust. Soc. Am. **105**, 1997–2009 (1999)]. The model calculation confirms many of the basic features in bubble dynamics observed experimentally, in particular the strong secondary shock wave emission generated by *in situ* lithotripter shock wave–inertial microbubble interaction. In addition, shock wave–inertial microbubble interaction produced by a Dornier HM-3, the most commonly used clinical lithotripter, was evaluated. It was shown that the forced collapse of inertial microbubbles with strong secondary shock wave emission could be produced consistently, provided that an appropriate preceding shock wave and interpulse delay were used. Further, it was demonstrated that truncation of the tensile stress of the lithotripter shock wave could significantly reduce the large expansion of the bubble following shock wave–inertial microbubble interaction, which may alleviate the risk for vascular injury during shock wave exposure. © 1999 Acoustical Society of America. [S0001-4966(99)01511-8]

PACS numbers: 43.80.Sh, 43.25.Yw [FD]

INTRODUCTION

To improve the efficiency of cavitation-mediated membrane permeabilization by lithotripter shock waves, we have recently developed a method of producing *in situ* shock wave–inertial microbubble interaction using a modified Dornier XL-1 lithotripter.¹ Briefly, inertial microbubbles are induced acoustically in an aqueous medium by a weak shock wave preceding the regular lithotripter pulse by a few microseconds. These microbubbles expand to a size of a few hundred microns before being collapsed *in situ* by the ensuing lithotripter pulse. This forced collapse of inertial microbubbles generates strong secondary shock wave emission and formation of microjets immediately behind the propagating lithotripter shock front. These unique features are absent from the dynamics of cavitation bubbles induced by standard lithotripter shock waves. With optimal combination of the preceding and lithotripter shock waves, membrane permeabilization of mouse lymphoid cells was found to be significantly enhanced at low exposure (50 shocks at 25 kV) while cell injury (defined as lysis and functional impairment of the cells) was substantially increased at high exposure (>100 shocks at 25 kV), compared to the standard lithotripter pulses.¹ Apparently, appropriate modification of the lithotripter waveform could dramatically alter the biological effect it produces.

To provide a theoretical perspective on the physical processes that may lead to a significantly altered bioeffect, we have studied the shock wave–inertial microbubble interaction using the Gilmore formulation for bubble dynamics coupled with zeroth-order gas diffusion, as originally described by Church.² First, we compared the dynamics of bubble oscillations produced by the various shock wave se-

quences investigated in our previous study.¹ The model calculations have confirmed qualitatively many of the characteristic features in bubble dynamics (except for microjet formation) produced by the modified XL-1 lithotripter. In particular, strong secondary shock wave emission due to the forced collapse of inertial microbubbles (70–250 μm in diameter at the moment of shock wave impingement) was predicted, which was found to be comparable to the shock wave emission generated by the inertial collapse of a much larger, millimeter-size bubble. Second, to identify the optimal preceding–lithotripter shock wave combination, we evaluated the effects of interpulse delay and the pressure amplitude of the preceding pulse on shock wave–inertial microbubble interaction. To ensure generality, the model calculation was carried out using a hypothetical modification of a Dornier HM-3 lithotripter, which is the most commonly used clinical lithotripter. It should be noted that two previous studies have examined the shock wave–inertial bubble interaction produced by two shock waves of similar pressure amplitudes with various phase combination and interpulse delay.^{3,4} However, in both studies gas diffusion across the bubble wall was not included in the model calculation. Furthermore, in this study modification of the tensile component of the lithotripter shock wave was explored theoretically to assess the possibility of minimizing vascular injury by reducing the large expansion of the rebound bubbles following shock wave–inertial microbubble interaction. Finally, bubble dynamics in response to inverted lithotripter shock waveforms were calculated and contrasted with that produced by the preceding–lithotripter shock wave combination.

I. METHODS

A. Gilmore formulation for bubble dynamics

The Gilmore formulation for bubble dynamics, coupled with zeroth-order gas diffusion, has been used previously by

^{a)}Electronic mail: pzl@me1.egr.duke.edu

TABLE I. Representative pulse parameters of the shock waves produced by the standard and modified Dornier XL-1 lithotripter at an output voltage of 25 kV.^a

Reflector configuration	Preceding shock wave			Lithotripter shock wave				
	P^+ (MPa)	P^- (MPa)	t^- (μ s)	P^+ (MPa)	P^- (MPa)	t^- (μ s)	α (s^{-1})	I_{index}^c
Standard				72.09	-19.81	4.32	0.878×10^6	3391
D2	3.36	-1.48	1.11	66.73	-22.76	1.83	1.868×10^6	1896
D3	3.33	-1.62 ^b	1.54	64.33	-17.91	3.70	1.061×10^6	2374
D6	6.03	-2.14	2.19	59.77	-12.38	3.36	1.412×10^6	1030

^aMaximum values (mean+s.d.) taken from previous measurements in Ref. 1.

^bValue interpolated linearly based on the corresponding values of D2 and D6 reflector configurations.

^c I_{index} is the mechanical index defined as $[P^-/\text{MPa}]^2 * [2 t^-/\mu\text{s}]$, which is roughly proportional to the mechanical work done to the bubble during the negative cycle of the lithotripter shock wave (see Ref. 18).

several groups to simulate the dynamics of cavitation bubbles in a lithotripter field.^{2,5} For conciseness, a detailed description of the theory is omitted here, but instead summarized in the Appendix. Two primary assumptions of the Gilmore formulation are that the bubble remains spherical in shape throughout the oscillation and the initial radius of the bubble is much smaller than the wavelength of the driving acoustic pulse. In our previous study,¹ it was observed via high-speed shadowgraph imaging that the forced collapse of the majority of the inertial microbubbles by the lithotripter pulse leads to strong secondary shock wave emission and spherically rebounded bubbles, features that are characteristic of symmetric collapse of the bubbles. However, the collapse of a few microbubbles of larger size appeared to be asymmetric, as indicated by the formation of microjets in the rebound bubbles. It was observed that the tendency of asymmetric collapse of the bubble during shock wave-inertial microbubble interaction increases with the size of the microbubble, although the threshold for such a transition from symmetric to asymmetric collapse was not established.¹ In addition, the estimated diameter of the inertial microbubble at the instance of lithotripter shock wave impingement is less than 250 μm [to be shown later in Fig. 5(b)], which is about an order of magnitude smaller than the lithotripter pulse length. Hence, a uniform pressure distribution around the microbubble, as assumed by the Gilmore formulation, is reasonably satisfied. Overall, on a qualitative basis, the Gilmore formulation appears to be appropriate to simulate the dynamics of an inertial microbubble impinged by a lithotripter shock wave.

B. Lithotripter fields

In this work, three different lithotripter fields were considered, namely, the modified XL-1 that was used in our previous study, the Dornier HM-3, which is the most commonly used clinical lithotripter, and an experimental electrohydraulic lithotripter with pressure-release reflector (to produce inverted lithotripter shock wave). As shown by Church,² the typical lithotripter shock wave (LSW) can be modeled by

$$P_s(t) = 2P^+ e^{-\alpha t} \cos(2\pi f t + \pi/3), \quad (1)$$

where $P_s(t)$ is the time history of the LSW, and we set $P_s(t) = 0$ for $t < 0$, P^+ is the peak positive pressure of the shock wave, α is the decay constant, and f is the frequency

determined by the negative pulse duration of the LSW, t^- , with $f = 1/(2t^-)$. Notice that the rise time of the shock front is not included in Eq. (1) since it has a minimal effect on the dynamics of LSW-induced bubble oscillations.⁵ In practice, it is usually convenient to substitute the values of P^+ and t^- measured experimentally into Eq. (1) and to adjust the value of α so that the best fit for the peak negative pressure, P^- , and the temporal profile of the LSW could be obtained.

As shown in Fig. 8 of Ref. 1, the modified XL-1 lithotripter produces, within 10 μs in front of the LSW, a preceding shock wave (PSW) and an intermediate shock wave (ISW). The PSW and ISW are generated, respectively, by wave diffraction and transmission through an annular ring reflector mounted on the aperture rim of the XL-1 reflector.¹ Using Eq. (1), the shock wave sequence produced by the modified XL-1 lithotripter in general can be described as

$$P_s = P_{\text{PSW}}(t) + P_{\text{ISW}}(t - \Delta t_{\text{PI}}) + P_{\text{LSW}}(t - \Delta t_{\text{PL}}), \quad (2)$$

where $P_{\text{PSW}}(t)$, $P_{\text{ISW}}(t)$ and $P_{\text{LSW}}(t)$ are the time history of the PSW, ISW, and LSW, whereas Δt_{PI} and Δt_{PL} are the interpulse delay between PSW and ISW, and between PSW and LSW, respectively. Based on previous measurements,¹ we chose $P_{\text{ISW}}^+ = P_{\text{PSW}}^+/4$, $\Delta t_{\text{PI}} = 4 \mu\text{s}$, and $\Delta t_{\text{PL}} = 9 \mu\text{s}$. In our previous study,¹ four different (standard and three modified, axisymmetric—D2, D3, and D6) reflector configurations were examined. The representative values of the P^+ , P^- , and t^- for the PSW and LSW, generated by the XL-1 lithotripter at 25 kV, as well as the α value for the best fit of LSW are summarized in Table I. Notice that the maximum values (defined as mean+s.d.) from the experimentally measured data were chosen. The reasons are twofold: (1) polyvinylidene difluoride (PVDF) membrane hydrophone tends to underestimate the tensile pressure of the LSW,⁶ and (2) enlargement of the electrode gap during shock wave lithotripsy (SWL) will increase the strength of the shock wave. Hence, a modeled shock wave based on the maximum values of the waveform parameters may be a better representative of the acoustic field used in the experiment, in which up to 250 shocks were delivered to a single sample,¹ and each electrode was used to produce a maximum of 1500 sparks at 25 kV. Figure 1 shows the modeled pressure waveforms of the shock wave sequences generated by the XL-1 lithotripter using the standard and the three modified reflector configurations, respectively. To facilitate comparison, each $P_s(t)$ curve was offset vertically except the bottom one, and, sub-

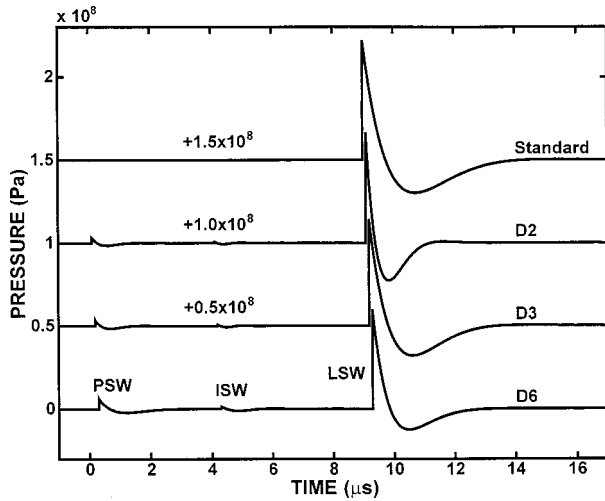


FIG. 1. Representative shock wave sequences generated by the original (or standard) and the modified Dornier XL-1 lithotripter with three different reflector configurations (D2, D3, and D6), modeled by Eq. (1) using pulse parameters listed in Table I.

sequently, this style of presentation was used throughout the paper.

For the shock wave produced by a standard HM-3 lithotripter,⁷ the typical pressure waveform is modeled by Eq. (1) with $P^+ = 40$ MPa, $P^- = -10$ MPa, and $t^- = -12$ μ s, using a best fit α of 7.03×10^5 s^{-1} . In order to reduce the large expansion of the rebound bubbles, we assume that an acoustic diode⁸ could be used to truncate the tensile pressure of the LSW below a threshold level, P_t^- . Such a modified pressure waveform can be described by Eq. (1) under the condition that $P_s(t)$ is set to equal to P_t^- when $P_s(t) < P_t^-$. Figure 2 illustrates a modeled pressure waveform generated by a HM-3 lithotripter with its tensile component truncated at $P_t^- = -5$ MPa.

To describe the shock waves generated by pressure-release reflectors, a time inverse lithotripter pressure waveform (a tensile wave followed by a compressive wave) is introduced as

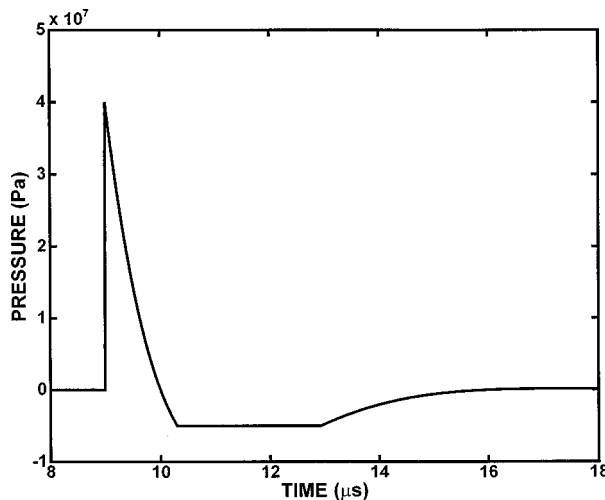


FIG. 2. Modeled pressure waveform of the shock wave generated by a Dornier HM-3 lithotripter with its tensile component truncated at -5 MPa.

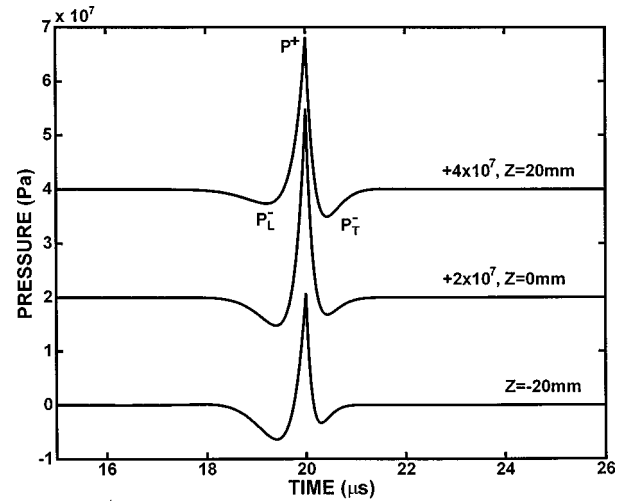


FIG. 3. Pressure waveforms of inverted lithotripter shock waves modeled using a combination of Eqs. (1) and (3), based on PVDF membrane hydrophone measurements taken at $z = -20, 0$, and 20 mm, respectively, along the major axis of an experimental electrohydraulic lithotripter (see Ref. 4).

$$P_s(t) = \begin{cases} 2P^+ e^{-\alpha(t_0-t)} \cos(2\pi f(t_0-t) + \pi/3), & 0 < t < t_0 \\ 0, & t < 0, t > t_0, \end{cases} \quad (3)$$

where t_0 denotes the time instance from which the waveform is horizontally inverted, and t_0 is larger than the total pulse duration of the LSW. Using a combination of Eqs. (1) and (3), an inverted LSW can be constructed with a leading tensile component, P_L^- , followed by a compressive component and a trailing tensile component, P_T^- . Figure 3 shows the modeled pressure waveforms of the inverted LSW, based on PVDF membrane hydrophone measurements taken at $z = -20, 0$ (F_2 —the external focus of the ellipsoidal reflector), and 20 mm along the major axis of an experimental electrohydraulic lithotripter equipped with a pressure-release reflector.⁴

C. Numerical algorithm and implementation

Notice that in response to a lithotripter pulse, the size of a bubble during its oscillation varies by several orders of magnitude.² Therefore, in order to reduce the numerical error in model computation, we have introduced the following dimensionless variables:

$$\begin{aligned} R' &= \frac{R}{R_0}, & t' &= \frac{t}{T_0}, & U' &= \frac{dR'}{dt'} = \frac{dR}{dt} \frac{T_0}{R_0}, \\ C' &= C \frac{T_0}{R_0}, & H' &= H \frac{T_0^2}{R_0^2}, \end{aligned} \quad (4)$$

and nondimensionalized the original Gilmore formulation [Eq. (A1)] to

$$\begin{aligned} R' \left(1 - \frac{U'}{C'} \right) \frac{dU'}{dt'} + \frac{3}{2} \left(1 - \frac{U'}{3C'} \right) U'^2 \\ = \left(1 + \frac{U'}{C'} \right) H' + \frac{1}{C'} \left(1 - \frac{U'}{C'} \right) R' \frac{dH'}{dt'}, \end{aligned} \quad (5)$$

where R_0 is the original bubble radius and T_0 is the reference time-scale for bubble oscillation. For convenience, T_0 is set to be $1 \mu\text{s}$.

The nondimensionalized Gilmore formulation (5) was then solved by using the fifth-order Runge–Kutta–Fehlberg method with a step-size control algorithm.⁹ To couple with gas diffusion [Eq. (A6)], an iterative method was used by first solving Eq. (5) with the initial number of moles of gas n_0 inside the bubble. The computed bubble response, $R(t)$, was then substituted into Eqs. (A6)–(A9) to determine a new number of moles of gas n inside the bubble, which, subsequently, was used to recalculate the bubble response curve. This computational process was repeated until the solution of n converges. The source code, written in MatLab Version 5 (The Mathworks Inc., Natick, MA), takes about 10 min to run a single simulation of the bubble response to lithotripter pulses on a Micron 166-MHz PC with Pentium processor and 32 MB RAM. The code was benchmarked against the calculations in Church's original paper² and excellent agreement was obtained.

Considering bubble oscillations in water, the values of the physical constants (see the Appendix for their definitions) used in the numerical calculations are $\rho_0 = 998 \text{ kg/m}^3$, $\mu = 1.046 \times 10^{-3} \text{ kg/m}\cdot\text{s}$, $\sigma = 72.583 \times 10^{-3} \text{ N/m}$, $C_l = 1500 \text{ m/s}$, $D = 2.42 \times 10^{-9} \text{ m}^2/\text{s}$, $P_0 = 1.01 \times 10^5 \text{ Pa}$, $C_0 = 0.7899 \text{ mol/m}^3$, $C_i/C_0 = 0.9$, $B = 3.039 \times 10^8 \text{ Pa}$, $\eta = 1.4$, and $n_0 = 6.9 \times 10^{-15} \text{ moles}$ (for $R_0 = 3 \mu\text{m}$). In this study, the initial radius of the bubble nucleus, R_0 , is set to be $3 \mu\text{m}$ for all cases.

II. RESULTS AND DISCUSSION

A. Modified XL-1 lithotripter

1. General characteristics

The response of a $3\text{-}\mu\text{m}$ cavitation nucleus, $R(t)$, to various XL-1 lithotripter-generated shock waves is shown in Fig. 4(a), in which R_{bi} denotes the radius of the bubble at the instance of shock wave–inertial microbubble (IMB) interaction. The typical response of the cavitation nucleus to a single shock wave (i.e., PSW or LSW) is an initial compression, a quick rebound and ensuing large expansion of the bubble, followed by an inertial collapse of the bubble and subsequent ringing. The maximum radius, R_{max} , and the collapse time, t_c , of the bubble increases with the peak value and duration of the tensile pressure of the incident shock wave (see, for example, the results of PSW versus LSW). Compared to the response to the LSW, the most significant difference in the response of the cavitation nucleus to the modified XL-1 shock waves, i.e., PSW+LSW or PSW+ISW+LSW, is the forced collapse of the inertial microbubbles (induced by PSW or PSW+ISW) by the LSW. Figure 4(b) shows the corresponding secondary shock wave emission in water at a radial distance of 5 mm from the bubble center, calculated by using Eq. (A10). The first peak pressure in water, P_{w1} , produced by the forced collapse of the microbubble in the case of PSW+(ISW+) LSW is significantly stronger than the corresponding value produced by the compression of the nucleus by the LSW. Also, two distinct subpeaks could be observed in the region of P_{w1} . We

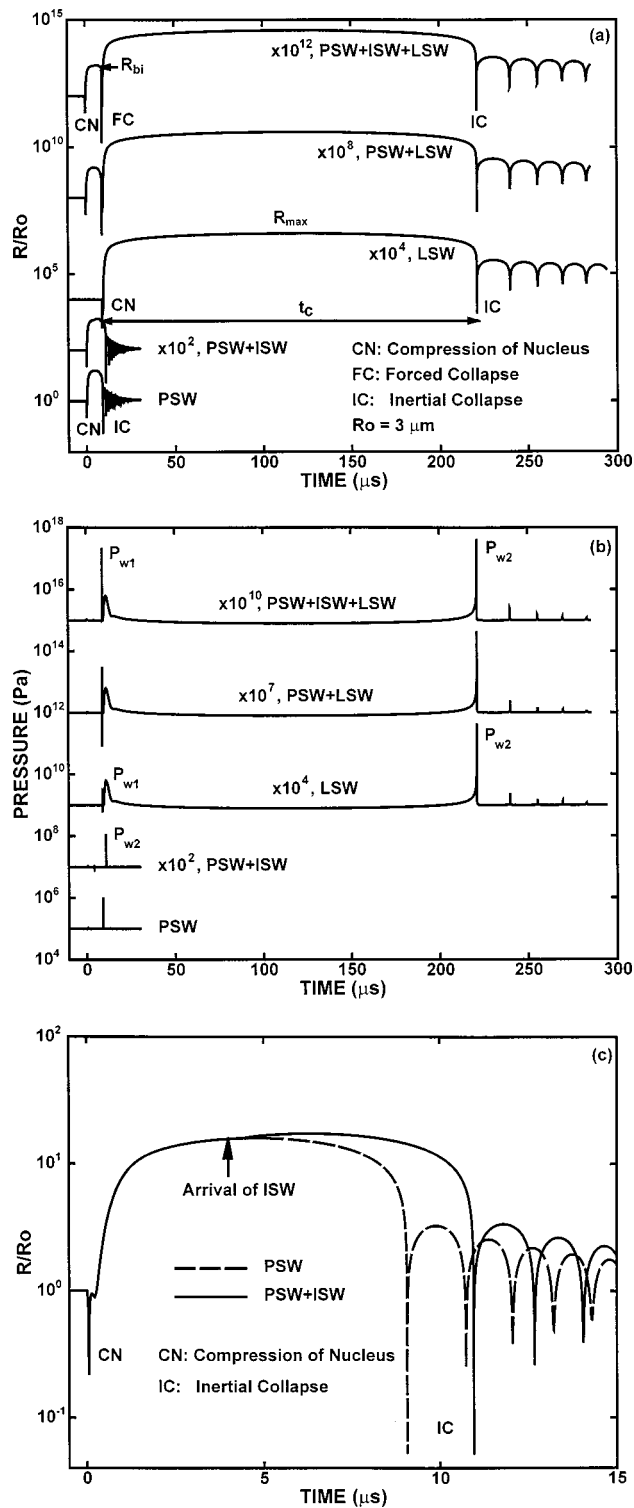


FIG. 4. Responses of a $3\text{-}\mu\text{m}$ cavitation nucleus to various combinations of shock waves produced by the modified Dornier XL-1 lithotripter with D3 reflector configuration. (a) Bubble radius normalized by the initial nucleus radius. (b) Corresponding secondary shock wave emission in water calculated at a radial distance of 5 mm from the bubble center. (c) Comparison of bubble response to PSW and PSW+ISW.

will refer the first peak P_{w1} to the higher of the two subpeaks, which correspond to the initial collapse and the subsequent rebound of the bubble, respectively. The second peak pressure in water, P_{w2} is produced by the inertial collapse of the bubble after its maximum expansion. Similar

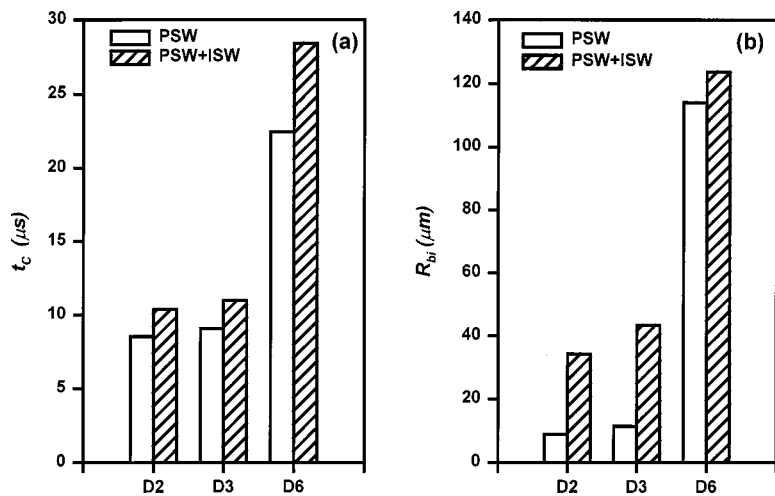


FIG. 5. The collapse time, t_c , shown in (a) and the size of the IMB at the instance of LSW impingement, R_{bi} , shown in (b) produced by PSW and PSW+ISW (bubble size at $t=9 \mu s$) with different reflector configurations. $R_0=3 \mu m$.

values of P_{w2} were obtained for both cases of LSW and PSW+(ISW+) LSW. This result suggests that P_{w2} is determined primarily by the tensile stress of the LSW,² and is minimally influenced by the bubble size at the instance of shock wave-IMB interaction, which is determined by PSW (+ISW). It is also worth noting that the interaction of ISW with the PSW-induced IMB does not produce a forced collapse of the microbubble, due to the relative weakness of the P^+ of the ISW [Fig. 4(c)]. Instead, the microbubble is only slightly compressed by the compressive stress, and subsequently further expanded by the tensile stress of the ISW to a larger size before the inertial collapse. The net effect of ISW, therefore, is to enlarge the size of the microbubble, and subsequently increases the momentum transfer during the LSW-IMB interaction.

2. Comparison of different reflector configurations

As shown in Fig. 5, when the pressure amplitude(s) of the PSW(+ISW) increases from D2 to D6 reflector configurations, the values of t_c and R_{bi} of the microbubbles increase accordingly. As noted earlier, the time delay between the PSW and LSW produced by the modified XL-1 lithotripter is about $9 \mu s$. Comparison of this interpulse time delay with the predicted value of t_c indicates that the LSW-IMB interaction is likely to occur in the collapsing phase of the IMB for

the D2 and D3 reflector configurations, but in the expansion phase of the IMB for the D6 reflector configuration. Further, it can be seen that the addition of ISW significantly increases the value of R_{bi} from that produced by PSW alone, in particular for the D2 and D3 reflector configurations. The predicted value of R_{bi} induced by PSW+ISW varies from 35 to $125 \mu m$, which is within the range ($<200 \mu m$) measured directly from high-speed photographic images in our previous study.¹

The predicted value of P_{w1} from the forced collapse of the microbubbles using the modified reflector is also much higher than the value produced by the initial compression of the cavitation nuclei by the standard LSW [Fig. 6(a)]. In addition, P_{w1} also increases from the D2 to the D6 reflector configuration, although the positive peak pressure of the corresponding LSW is decreasing in this order (see Table I). This result suggests that R_{bi} is the primary determinant for P_{w1} , provided that LSW is sufficiently strong. The fact that P_{w1} increases significantly from PSW+LSW to PSW+ISW+LSW for the D2 and D3, but not for the D6 reflector configuration further supports this conclusion. In addition, the predicted values of P_{w2} for the modified reflectors are almost identical between LSW and PSW(+ISW)+LSW [Fig. 6(b)], indicating again that P_{w2} is determined primarily by the tensile strength of the LSW, or,

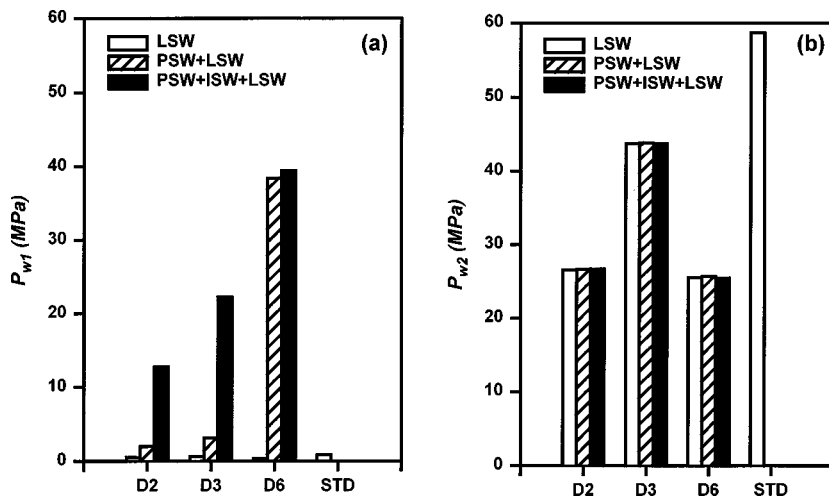


FIG. 6. Comparison of peak pressure produced in water by different reflector configurations and shock wave sequences. (a) P_{w1} and (b) P_{w2} . $R_0=3 \mu m$.

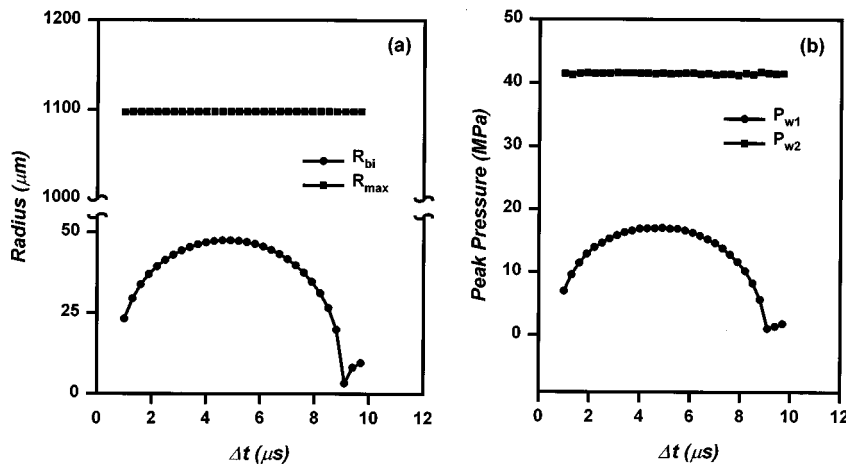


FIG. 7. Effect of interpulse delay, Δt , on (a) bubble radii and (b) secondary shock wave emissions produced by a modified HM-3 lithotripter. $R_0 = 3 \mu\text{m}$.

more precisely, the mechanical work done on the bubble by the tensile stress of the LSW. The prediction that P_{w2} is larger for the D3 than for the D2 and D6 reflector configurations, and the largest value is produced by the standard reflector configuration further corroborates theoretically with this speculation (see Table I for the values of the mechanical index of the LSWs). It is also interesting to note that the predicted value of P_{w1} is smaller than P_{w2} for the D2, D3, and standard reflector configurations, but larger than P_{w2} for the D6 reflector configuration, which induces the largest microbubbles (Figs. 5 and 6). This prediction is consistent with the results of acoustic emission measurements from the modified XL-1 lithotripter.¹

B. HM-3 lithotripter

To assess the optimal condition for producing desirable shock wave-IMB interaction, we have considered a hypothetical modification of the most widely used clinical lithotripter, the Dornier HM-3. We assume that the criterion for optimal combination of PSW and LSW is to produce the strongest forced collapse of IMB, which could be associated with the mechanical stresses that generate bioeffects. Further, we assume that following the concept described and tested in our previous study,¹ a similar modification of the ellipsoidal reflector of a HM-3 lithotripter could be made. For simplicity, we considered the addition of a PSW in front of the standard LSW produced by the HM-3. The ISW was omitted to simplify the model calculation, and, physically, it can be eliminated by acoustic masking. Three factors that may influence LSW-IMB interaction and the resultant bubble dynamics were considered, as described in the following.

1. Effect of interpulse delay between PSW and LSW

First, we evaluated the effect of interpulse delay between PSW and LSW, Δt , on the resultant bubble radii (R_{bi} and R_{max}) and the secondary shock wave emissions (P_{w1} and P_{w2}) generated by the collapse of the bubble. In the following, PSW was assumed to be the one produced by the XL-1 lithotripter at 25 kV using the D3 reflector configuration (see Table I), unless otherwise specified. The LSW was modeled by Eq. (1) with $P^+/P^- = 40/-10$ MPa, and $t^- = -12 \mu\text{s}$, as described previously. For a given combination of PSW and

LSW, it was predicted that there is an optimal Δt at which maximum values of R_{bi} and P_{w1} could be obtained (Fig. 7). This optimal interpulse delay corresponds to the time needed for the inertial microbubble induced by the PSW to expand to its maximum size before being collapsed by the ensuing LSW, a condition that would ensure maximum momentum transfer during the LSW-IMB interaction. Similar results were also obtained in previous studies using two shock waves of different phase combination and interpulse delay.^{3,4} On the other hand, the interpulse delay has no effect on R_{max} and P_{w2} , which are determined solely by the tensile strength of the LSW. It can also be noted that near the optimal value of Δt , the variations of R_{bi} and P_{w1} with respect to Δt are almost symmetric. Moreover, it should be pointed out that the forced collapse of the inertial microbubble could be produced within a range around the optimal Δt , despite the fact that under those conditions the interaction would occur at a smaller bubble size. As shown in Fig. 7, even with 50% variation of Δt around its optimal value, the corresponding decrease in P_{w1} (from 17.0 to 13.8 MPa) is less than 19%, and these pressure peaks are an order of magnitude higher than that (0.42 MPa) produced by the initial compression of the cavitation nuclei by LSW alone. This result indicates that with appropriate Δt , LSW-IMB interaction could produce forced collapse of inertial microbubbles in a volume around the lithotripter focus, as observed experimentally in our previous study.¹

2. Effect of PSW

Second, we evaluated the effect of PSW on LSW-IMB interaction. While maintaining a constant ratio of $P^+/P^- = 2.06$, we varied the peak positive pressure of the PSW, P_{PSW}^+ , and calculated the corresponding bubble dynamics and resultant acoustic emission. For each case, we used the optimal Δt between the PSW and LSW so that maximum values of R_{bi} and P_{w1} were obtained. The results show that R_{bi} and P_{w1} increase almost linearly with P_{PSW}^+ while the corresponding values of R_{max} and P_{w2} remain unchanged (Fig. 8). Most interestingly, the calculations predict that when P_{PSW}^+ exceeds 9.7 MPa, P_{w1} will become greater than P_{w2} , despite the fact that the corresponding value of R_{bi} (which leads to P_{w1} due to forced collapse) is an order of magnitude smaller than R_{max} (which leads to P_{w2} due to

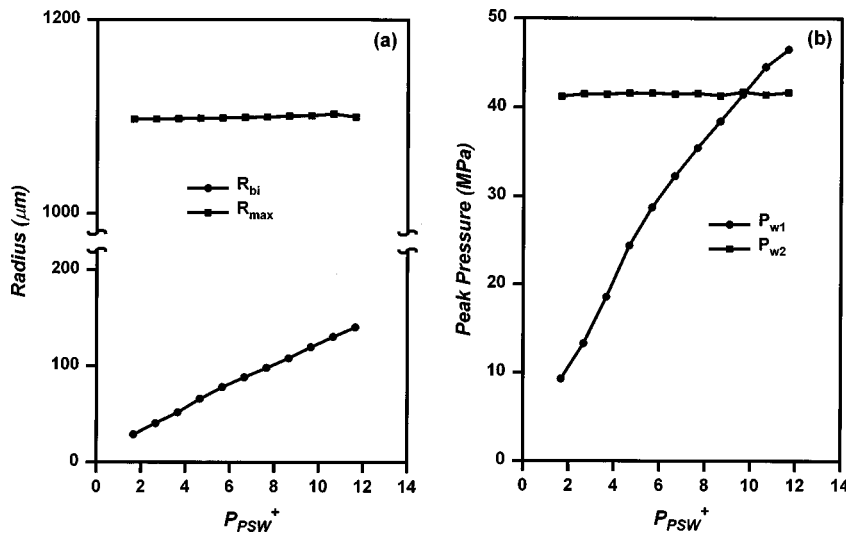


FIG. 8. Effect of preceding shock wave on (a) bubble radii and (b) secondary shock wave emissions produced by a modified HM-3 lithotripter. The interpulse delay, Δt , is set at the optimal value. $R_0 = 3 \mu\text{m}$.

inertial collapse). This result clearly demonstrates the potential of using forced collapse of inertial microbubbles to produce strong bubble collapse *in vivo*, such as in blood vessels where the fluid-filled space is quite limited. In contrast to the model prediction of bubble dynamics *in vitro*, the expansion of LSW-induced cavitation bubbles *in vivo* could be severely hindered by surrounding tissue structure, resulting in non-spherical bubble deformation. Consequently, the violence of the subsequent inertial collapse of the bubble and the corresponding P_{w2} *in vivo* would be greatly reduced. This could be a primary reason for the general observation that the bioeffect produced by standard LSW *in vivo* is much less significant than that produced *in vitro*.¹⁰ In contrast, the forced collapse of microbubbles capable of generating strong shock wave emission (and associated mechanical stresses) in limited fluid-filled space could have unique advantages for producing desirable biological effects *in vivo*. Further *in vivo* studies are needed to explore this unique property of the shock wave-IMB interaction.

3. Effect of truncated P_{LSW}^-

In vivo, the large expansion of LSW-induced cavitation bubbles is not only constrained by the surrounding tissue structure, it may also cause rupture of capillary and small blood vessels.¹¹ Thus, we further hypothesize that the optimal preceding-lithotripter shock wave sequence for effective and safe macromolecule delivery *in vivo* would be the one in which the LSW has a significantly reduced tensile component. To achieve this, an acoustic filter that can selectively reduce the tensile stress of the LSW, P_{LSW}^- , without significantly affecting the compressive pressure of the LSW is needed. Such an acoustic filter (or diode) was proposed by Riedlinger in 1989,⁸ although its application to lithotripsy has not been reported. If we assume such an acoustic diode could be constructed for an HM-3 lithotripter, the impact on LSW-induced bubble expansion would be quite significant based on our model calculation. As shown in Fig. 9, theoretically when P_{LSW}^- is truncated from -10 to -0.5 MPa, the corresponding value of R_{max} and P_{w2} would drop monotonically from 1100 to $120 \mu\text{m}$ and from 41 to 4 MPa, respectively. This significant reduction in the maximum expansion

of LSW-induced bubbles would greatly reduce the potential for vascular injury *in vivo* due to intraluminal bubble expansion.¹¹ Further experiments should be carried out to test this hypothesis.

C. Electrohydraulic lithotripter with pressure-release reflectors

Shock wave-IMB interaction may also be induced by inverted lithotripter shock waves (ILSW), which has a leading tensile component followed by a compressive wave.¹² Michael Bailey has described a method of using pressure-release reflector inserts inside an electrohydraulic lithotripter for the generation of ILSW.⁴ Except for the inversion of the waveform, the ILSW has similar peak pressures, pulse duration, and acoustic energy compared to the standard LSW. However, because of the waveform inversion, cavitation activity is significantly suppressed, and minimal injury is produced in cells and renal tissue exposed to ILSW.^{13,14} In the following, we will examine the basic features in bubble dy-

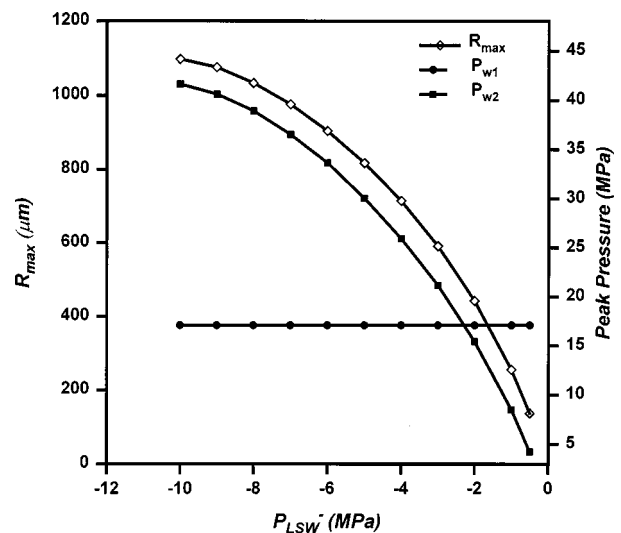


FIG. 9. Effect of truncation of the tensile pressure of LSW on maximum bubble radius and secondary shock wave emissions produced by a modified HM-3 lithotripter. $R_0 = 3 \mu\text{m}$.

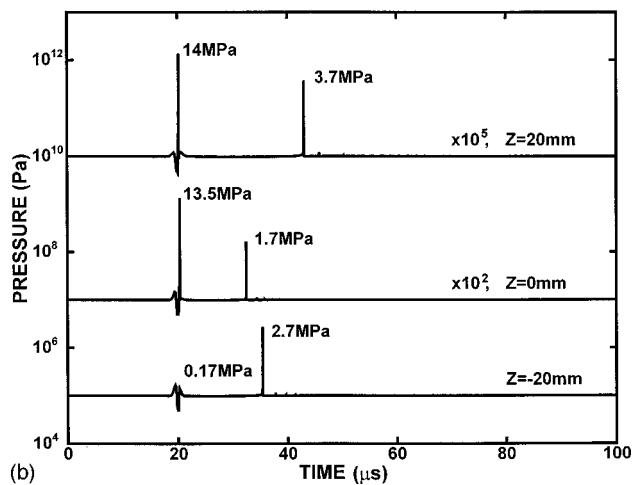
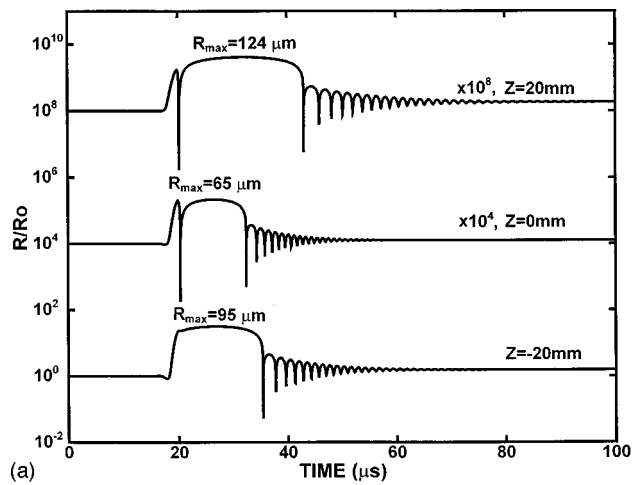


FIG. 10. Responses of a $3\text{-}\mu\text{m}$ cavitation nucleus to inverted lithotripter shock waves at three different positions along the axis of an experimental electrohydraulic lithotripter with pressure-release reflector (see Ref. 4). (a) Bubble radius normalized by the initial nucleus radius. (b) Corresponding secondary shock wave emissions in water calculated at a radial distance of 5 mm from the bubble center.

namics produced by ILSW and compare them with that produced by preceding-lithotripter shock wave combination.

Figure 10(a) shows the predicted bubble response of a $3\text{-}\mu\text{m}$ nucleus to the three different ILSWs (see Fig. 3) measured at $z = -20, 0$ (F_2), and 20 mm along the major axis of an experimental electrohydraulic lithotripter equipped with a pressure-release reflector.⁴ It can be seen that the bubble response is quite sensitive to the ratio of the leading peak negative pressure, P_L^- , to the ensuing peak compressive pressure P^+ of the wave (see also Fig. 3). When the ratio of P_L^-/P^+ is high, such as in the case of pressure waveform at $z = -20$ mm, the nuclei is first expanded by a strong leading tensile wave, and then the outward motion of the bubble is quickly slowed down by the ensuing compressive wave. However, because the initial expansion of the bubble is so strong, the compressive wave could only slightly reverse the motion of the bubble, but cannot force the bubble to collapse completely before the trailing tensile wave (P_T^-) reexpands the bubble again. On the other hand, for the pressure waveforms at $z = 0$ and 20 mm where the ratio of P_L^-/P^+ is low, the initial expansion of the bubble is not so strong that the

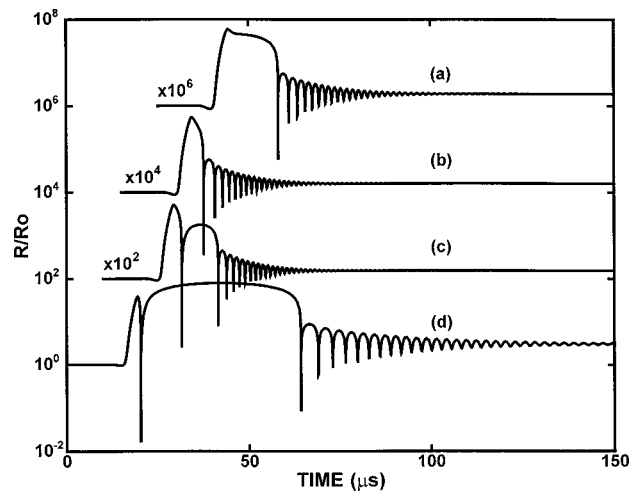


FIG. 11. Effect of the leading tensile pressure of ILSW, P_L^- , on bubble dynamics. The corresponding values of P_L^- are (a) -10 MPa, (b) -9 MPa, (c) -8.5 MPa, and (d) -6 MPa, respectively. In all four cases, $P^+/P_T^- = 40/-3.85$ MPa were used. Notice the transition from forced to nonforced collapse of the bubble at $P_L^- = -9$ MPa [see curve (b)]. $R_0 = 3 \mu\text{m}$.

ensuing compressive wave is sufficient to reverse the outward motion of the bubble, leading to a forced collapse of the bubble before its reexpansion by P_T^- . Correspondingly, the calculated shock wave emission (P_{w1}) in water is much higher for the bubble(s) with forced collapse than that without forced collapse [Fig. 10(b)]. The transition from forced collapse to nonforced collapse is clearly illustrated in Fig. 11 where P_L^- is hypothetically increased from -6 to -10 MPa while P^+ and P_T^- are kept unchanged. Initially, when P_L^- is relatively small, a forced collapse of the bubble is produced, followed immediately by a large reexpansion and then an inertial collapse of the bubble with subsequent ringing. As P_L^- becomes stronger, the forced collapse of the bubble becomes weaker, and the duration of the bubble reexpansion decreases. Eventually, when P_L^- approaches a critical value of -9 MPa, the forced collapse disappears, and only the inertial collapse is predicted after a time delay. Further increase of P_L^- will lengthen the time delay to the inertial collapse.

In comparison to the bubble dynamics generated by optimal preceding-lithotripter shock wave combination whereby forced collapse of an IMB is always produced, the bubble dynamics from ILSW is less consistent, and forced collapse of IMBs may not always occur. More importantly, the shock wave-IMB interaction produced by ILSW does not occur at the optimal phase of the IMB oscillation, as discussed previously.¹ This can be seen clearly by comparing the results in Fig. 10(b) (produced by ILSW) with those in Fig. 8(b) (from preceding-lithotripter shock wave combination). For a comparable preceding tensile wave, if the appropriate time delay were allowed for the IMB to grow to its maximum size before the LSW-IMB interaction, a significantly stronger P_{w1} would be generated. On the other hand, in general the maximum expansion of the bubble induced by ILSW is significantly reduced compared to that produced by a standard LSW. This feature, combined with the observation that minimal vascular injury is produced by ILSW in renal tissue, seems to corroborate the theory that intraluminal

bubble expansion is a primary mechanism for vascular injury during lithotripsy.¹¹

III. CONCLUSIONS

The Gilmore model coupled with zeroth-order gas diffusion was used to simulate the bubble dynamics generated by various shock wave sequences of a modified XL-1 lithotripter. The results show that LSW-IMB interaction can generate strong secondary shock wave emission comparable to that produced by the inertial collapse of a much larger, millimeter-size bubble. The model prediction also confirms many of the features of bubble dynamics observed experimentally, in particular for bubble dynamics produced by different reflector configurations. This method was then extended to identify the optimal combination of preceding and lithotripter shock waves for producing the most desirable LSW-IMB interaction using a Dornier HM-3 lithotripter. The model calculation suggests that with appropriate PSW and interpulse delay between the PSW and LSW, the forced collapse of IMBs with strong secondary shock wave emission can be produced within a volume around the lithotripter focus. Further, it was demonstrated that truncation of the tensile stress of LSW could significantly reduce the large expansion of the bubble following LSW-IMB interaction, which may lessen the risk for vascular injury during shock wave exposure.

ACKNOWLEDGMENTS

This work was supported in part by NIH through Grant Nos. R21-HL60327, RO1-DK52985, and PO1-DK20543.

APPENDIX: THE GILMORE FORMULATION FOR BUBBLE DYNAMICS²

Considering the compressibility of the liquid, the radial oscillation of a single spherical bubble can be described by the original Gilmore formation:¹⁵

$$R \left(1 - \frac{U}{C} \right) \frac{dU}{dt} + \frac{3}{2} \left(1 - \frac{U}{3C} \right) U^2 = \left(1 + \frac{U}{C} \right) H + \frac{1}{C} \left(1 - \frac{U}{C} \right) R \frac{dH}{dt}, \quad (A1)$$

where R is the bubble radius, $U (= dR/dt)$ is the velocity of the bubble wall, and C and H are the speed of sound in the liquid at the bubble wall and the enthalpy difference between the liquid at pressure $P(R)$ and pressure P_∞ , respectively, which are determined by

$$H = \int_{P_\infty}^{P(R)} \frac{dP}{\rho}, \quad (A2)$$

$$C = [C_l^2 + (m-1)H]^{1/2}, \quad (A3)$$

where P and ρ are the time-varying pressure and density of liquid, P_∞ is the pressure at infinity, C_l is the infinitesimal speed of sound in the liquid, and m is a constant. When a lithotripter shock wave P_S is produced in the liquid far away from the bubble, we have $P_\infty = P_0 + P_S$ where P_0 is the ambient pressure of the surrounding liquid. To determine H and

C , the equation of state for a compressible fluid (Tait equation) and the pressure at the bubble wall, $P(R)$, in relation to the gas pressure inside the bubble (P_g), liquid viscosity (μ), and surface tension (σ) in the liquid are considered and given in the following,

$$P = A(\rho/\rho_0)^m - B, \quad (A4)$$

$$P(R) = P_g - \frac{2\sigma}{R} - \frac{4\mu}{R} U, \quad (A5)$$

where ρ_0 is the equilibrium liquid density, and $A = C_l^2 \rho / P_0 m$ with $m=7$ and $B=A-1$.

The instantaneous number of moles of gas n in a bubble may be calculated from the zeroth-order solution to the diffusion equation given by Eller and Flynn:¹⁶

$$n = n_0 - 4(\pi D)^{1/2} \int_0^\tau F(\tau') (\tau - \tau')^{-1/2} d\tau', \quad (A6)$$

where D is the diffusion constant of the gas in the liquid, n_0 is the number of moles of gas initially present in the bubble, and

$$\tau = \int_0^t R^4(t') dt', \quad (A7)$$

$$F(\tau) = C_0(P_g/P_0) - C_i, \quad (A8)$$

where

$$P_g = \left(P_0 + \frac{2\sigma}{R_0} \right) \frac{n}{n_0} \left(\frac{R_0}{R} \right)^{3\eta} \left(\frac{R_{0n}}{R_0} \right)^{3(\eta-1)}, \quad (A9)$$

R_0 is the initial equilibrium radius of the bubble, $R_{0n}(t)$ is the time-varying equilibrium bubble radius, η is the polytropic exponent of the gas, C_0 is the saturation concentration of the gas in the liquid, and C_i is the initial concentration of the gas in the liquid far from the bubble.

As described by Akulichev,¹⁷ the pressure distribution in the liquid at a distance r from the bubble center is given by

$$P_r(t) = A \left[\frac{2}{m+1} + \frac{m-1}{m+1} \left(1 + \frac{m+1}{rC_l^2} G \right)^{1/2} \right]^{2m/(m-1)} - B, \quad (A10)$$

where G is an invariant of the bubble motion that may be specified at the bubble surface by

$$G = R(H + U^2/2). \quad (A11)$$

¹P. Zhong, H. F. Lin, X. F. Xi, S. L. Zhu, and E. S. Bhogte, "Shock wave-inertial microbubble interaction: Methodology, physical characterization, and bioeffect study," J. Acoust. Soc. Am. **105**, 1997-2009 (1999).

²C. C. Church, "A theoretical study of cavitation generated by an extracorporeal shock wave lithotripter," J. Acoust. Soc. Am. **86**, 215-227 (1989).

³Z. Ding and S. M. Gracewski, "Response of constrained and unconstrained bubbles to lithotripter shock wave pulses," J. Acoust. Soc. Am. **96**, 3636-3644 (1994).

⁴M. R. Bailey, "Control of acoustic cavitation with application to lithotripsy," Ph.D. dissertation, Univ. of Texas at Austin, May 1997.

⁵M. J. Choi, A. J. Coleman, and J. E. Saunders, "The influence of fluid properties and pulse amplitude on bubble dynamics in the field of a shock wave lithotripter," Phys. Med. Biol. **38**, 1561-1573 (1993).

⁶J. Staudenraus and W. Eisenmenger, "Fiber-optic probe hydrophone for

- ultrasonic and shock-wave measurements in water," *Ultrasonics* **31**, 267–273 (1993).
- ⁷A. J. Coleman and J. E. Saunders, "A survey of the acoustic output of commercial extracorporeal shock wave lithotripters," *Ultrasound Med. Biol.* **15**, 213–227 (1989).
- ⁸R. Riedlinger, "Acoustic diode," U.S. Patent 4618796 (1989).
- ⁹J. R. Rice, *Numerical Methods, Software, and Analysis* (Academic, San Diego, 1993), pp. 421–426.
- ¹⁰M. Delius, "Medical applications and bioeffects of extracorporeal shock waves," *Shock Waves* **4**, 55–72 (1994).
- ¹¹P. Zhong, I. Cioanta, S. L. Zhu, F. H. Cocks, and G. M. Preminger, "Effects of tissue constraint on shock wave-induced bubble expansion *in vivo*," *J. Acoust. Soc. Am.* **104**, 3126–3129 (1998).
- ¹²M. Mueller, "Experimental investigations on focusing of weak spherical shock waves in water by shallow ellipsoidal reflectors," *Acustica* **64**, 85–93 (1987).
- ¹³B. Jordan, M. R. Bailey, R. O. Cleveland, and L. A. Crum, "Detection and control of lithotripsy-induced cavitation in blood," *Proceedings of the 16th International Congress on Acoustics and 135th meeting of the Acoustical Society of America*, Vol. 4, pp. 2809–2810 (1998).
- ¹⁴A. P. Evan, L. R. Willis, B. A. Connors, J. A. McAteer, J. E. Lingeman, R. O. Cleveland, M. R. Bailey, and L. A. Crum, "Separation of cavitation and renal injury induced by shock wave lithotripsy (SWL) from SWL-induced impairment of renal hemodynamics," *Proceedings of the 16th International Congress on Acoustics and 135th meeting of the Acoustical Society of America*, Vol. 4, pp. 2487–2488 (1998).
- ¹⁵F. R. Gilmore, *The Growth or Collapse of a Spherical Bubble in a Viscous Compressible Liquid* (California Institute of Technology, Pasadena, CA, 1952), Report No. 26-4, pp. 1–40.
- ¹⁶A. Eller and H. G. Flynn, "Rectified diffusion during nonlinear pulsations of cavitation bubbles," *J. Acoust. Soc. Am.* **37**, 493–501 (1965).
- ¹⁷V. A. Akulichev, in *High-Intensity Ultrasonic Fields*, edited by L. D. Rozenberg (Plenum, New York, 1971), pp. 203–259.
- ¹⁸T. G. Leighton, *The Acoustic Bubble* (Academic, London, 1994), pp. 329–332.